A compact Incoherent Broadband Cavity Enhanced Absorption Spectrometer (IBBCEAS) for trace detection of nitrogen oxides, iodine oxide and glyoxal at sub-ppb levels for field application

Albane Barbero[1], Camille Blouzon[1], Joël Savarino[1], Nicolas Caillon[1], Aurélien Dommergue[1], and Roberto Grilli[1]

[1]Univ. Grenoble Alpes, CNRS, IRD, Grenoble INP*, IGE, 38000 Grenoble, France
*Institute of Engineering Univ. Grenoble Alpes

Correspondence: Roberto Grilli (roberto.grilli@cnrs.fr)

Abstract. We present a compact, affordable and robust instrument based on Incoherent Broadband Cavity Enhanced Absorption Spectroscopy (IBBCEAS) for simultaneous detection of NO_x, IO, CHOCHO and O_3 in the 400 – 475 nm wavelength region. The instrument relies on the injection of a high-power LED source in a high-finesse cavity (F ∼ 33,100), with the transmission signal be detected by a compact spectrometer based on a high-order diffraction grating and a CCD camera. A minimum detectable absorption of 2.0×10^{-10} cm^{-1} was achieved within ∼ 22 minutes of total acquisition, corresponding to a figure of merit of 1.8×10^{-10} cm^{-1} Hz$^{-1/2}$ per spectral element. Due to the multiplexing broadband feature of the setup, multi-species detection can be performed with simultaneous detection of NO_2, IO, CHOCHO, and O_3 achieving detection limits of 11, 0.3, 10 ppt and 47 ppb (1σ) within 22 min of measurement, respectively (half of the time spent on the acquisition of the reference spectrum in absence of absorber, and the other half on the absorption spectrum). The implementation on the inlet gas line of a compact ozone generator based on electrolysis of water allows the measurement of NO_x (NO + NO_2) and therefore an indirect detection of NO with detection limits for NO_x and NO of 10 and 21 ppt (1σ), respectively. The device has been designed to fit in a 19", 3U rack-mount case, weights 15 kg and has a total electrical power consumption < 300 W. The instrument can be employed to address different scientific objectives such as better constraint the oxidative capacity of the atmosphere, study the chemistry of highly reactive species in atmospheric chambers as well as in the field, and looking at the sources of glyoxal in the marine boundary layer to study possible implications on the formation of secondary aerosol particles.

1   Introduction

Free radicals are controlling the oxidative capacity of the atmosphere and therefore contribute to the upholding of its chemical balance. With their unpaired valence electron, they are highly chemically reactive, and are therefore considered the "detergents" of the atmosphere (Monks, 2005; Monks et al., 2009). Even if present at extremely low concentrations, radicals are constantly formed by photochemical and combustion processes. They may be removed from the atmosphere by biological uptakes, dry and wet deposition, and chemical reactions (Finlayson-Pitts and Pitts, 2000). Free radicals in the troposphere such as nitrogen oxides (NO_x), hydroxyl radical (OH), peroxy radicals (HO_2, RO_2) and halogen oxides (BrO and IO), can be found

at mixing ratios (i.e. mole fractions) ranging from less than one part per trillion (10^{-12} mol mol^{-1} or ppt) up to a few parts per million (10^{-6} mol mol^{-1} or ppm) in the atmosphere (Wine and Nicovich, 2012). Measuring their concentration and dynamic

25   variability in different atmospheric environments is key for addressing specific questions regarding air quality, the oxidative state of the atmosphere, the ozone budget, aerosol nucleation, as well as carbon, nitrogen and sulfur cycles. The understanding of the complex interactions involving those species has led to numerous investigations during the past decades. Especially, nitrogen oxides (NO_x = NO and NO_2), have a direct impact on air quality and climate change. In presence of volatile organic compounds (VOCs) and under solar radiation, nitrogen oxides stimulate ozone (O_3) formation in the troposphere. NO_x also

30   plays an important role in rain acidification and ecosystems eutrophication by its transformation in nitric acid (HNO_3) (Jaworski et al., 1997; Vitousek et al., 1997). Finally, NO_x contribute to the formation of particulate matter in ambient air and to the aerosol formation leading to clouds formation (Atkinson, 2000). The NO_2 mixing ratio in the troposphere ranges from a few tens of ppt in remote areas to hundreds of ppb (10^{-9} mol mol^{-1}) in urban atmospheres (Finlayson-Pitts and Pitts, 2000). Being able to measure such species in situ, at low levels and at a time scale compatible with its reactivity (i.e. in min) is

35   challenging and puts stringent constraints on the instrument sensitivity, time response, energy consumption and compactness. Among the various techniques that have so far been developed, ChemiLuminescence Detection (CLD) (Maeda et al., 1980; Ryerson et al., 2000), Long-Path Differential Optical Absorption Spectroscopy (LP-DOAS) (Lee et al., 2005; Pikelnaya et al., 2007; Lee et al., 2008), and Multi-AXis Differential Optical Absorption Spectroscopy (MAX-DOAS) (Platt and Perner, 1980; Sinreich et al., 2004; Wagner et al., 2010) have been used to detect nitrogen species and halogen oxides. The CLD technique,

40   using the chemiluminescence reaction occurring between O_3 and NO after the reduction of NO_2 into NO, is widely used for air quality measurements with sensitivities better than 100 ppt (Ryerson et al., 2000). Nevertheless, the interferences in the reduction of NO_2 to NO with other species (i.e. HONO, HNO_3) and the sensitivity to environmental conditions (temperature and humidity) leave uncertainties on absolute mixing ratio measurements (Grosjean and Harrison, 1985; Williams et al., 1998). The MAX-DOAS technique has been used to measure BrO and NO_2 by making use of the characteristic absorption features of

45   gas molecules along a path in the open atmosphere (Leser et al., 2003). Although MAX-DOAS is relatively simple to deploy, the data analysis makes it a complex approach for in situ field measurements due to the influence of clouds on the radiative transfer which alters the path length of light (Wittrock et al., 2004; Rozanov and Rozanov, 2010). While in LP-DOAS the optical path length is known, the signal degradation due to the environment (clouds, rain, wind) remains of importance for the data retrieval and results are integrated over the long path leading to a limited spatial resolution (Chan et al., 2012; Pöhler et al.,

50   2010). Compact, high sensitive and point-source measurements may be achieved using cavity enhanced techniques such as Cavity Ring Down Spectroscopy (CRDS) and Cavity Enhanced Absorption Spectroscopy (CEAS) (Atkinson, 2003). The potential of the CRDS for accurate, sensitive and rapid measurements in a compact and transportable instrument has already been demonstrated (Fuchs et al., 2009; Brown et al., 2002), e.g. Fuchs et al. (2009) reached a sensitivity of 22 ppt for NO_2 within 1 s of integration time using the CRDS technique. Incoherent Broadband Cavity Enhanced Absorption Spectroscopy (IBBCEAS)

55   (Fiedler et al., 2003) is a simple and robust technique for in situ field observations. Different sources and wavelength regions have been used for the detection of NO_2 leading to different performances: Venables et al. (2006) were able to detect simultaneously NO_3, NO_2, O_3 and H_2O in an atmospheric simulation chamber with a sensitivity of tens of ppb for NO_2 ; Gherman

et al. (2008) reached ~ 0.13 ppb and ~ 0.38 ppb for HONO and NO_2 in a 4 m^3 atmospheric simulation chamber between 360 and 380 nm ; Triki et al. (2008) used a red LED source centered at 643 nm reaching a sensitivity of 5 ppb ; Langridge et al.

60 (2006) developed an instrument with a blue light emitting diode (LED) centered at 445 nm allowing detection limits ranging from 0.1 to 0.4 ppb ; Ventrillard-Courtillot et al. (2010) reached 600 ppt detection limit for NO_2 with a LED centered at 625 nm ; while Thalman and Volkamer (2010) reported a detection limit of 30 ppt within 1 min of integration time. More recently, Min et al. (2016) proved a precision of 80 ppt in 5 s of integration at 455 nm using a spectrometer with a thermoelectric cooled CCD camera and very high reflective mirrors. This non-exhaustive list of works underline the need of robust, compact

65 and transportable instruments also allowing direct multi-species detection and low detection limits for applications in remote areas such as Antarctica, where the expected mixing ratio of NO_2 could be as low as a few tens of ppt. Fuchs et al. (2010), during the NO$_3$Comp campaign at the SAPHIR atmospheric simulation chamber, demonstrated the potential of theses optical techniques to compete with the CLD instruments as routine measurements of NO_2 concentrations in the future. The present paper describes a compact and affordable instrument based on the IBBCEAS technique, allowing the simultaneous detection

70 of nitrogen dioxide, iodine oxide, glyoxal and ozone (NO_2, IO, CHOCHO and O_3), with detection limits of 11, 0.3, 10 ppt and 47 ppb (1σ), respectively, for a measurement time of 22 min (half of the time spent on the acquisition of the reference spectrum in absence of absorber, and the other half on the absorption spectrum). The four species are directly detected by a broadband blue light emitting diode centered at 445 nm. The wavelength region was selected in order to optimize the detection of NO_2. Direct detection of NO is only possible in UV region for wavelengths around 226 nm (Dooly et al., 2008) or in the mid-infrared

75 region at 5.3 μm (Richard et al., 2018), wavelengths difficult to achieve with LED technology. Here, an indirect measurement is proposed which relies on the oxidation of NO to NO_2 under a controlled excess of O_3. The sum of NO and NO_2 is therefore measured leading to a supplemental indirect measurement of NO if concentration of NO_2 is also monitored. The field deployment for the measurements of NO_2 and NO_x consists of two twin instruments, IBBCEAS-NO_2 and IBBCEAS-NO_x, the later equipped with an ozone generator system.
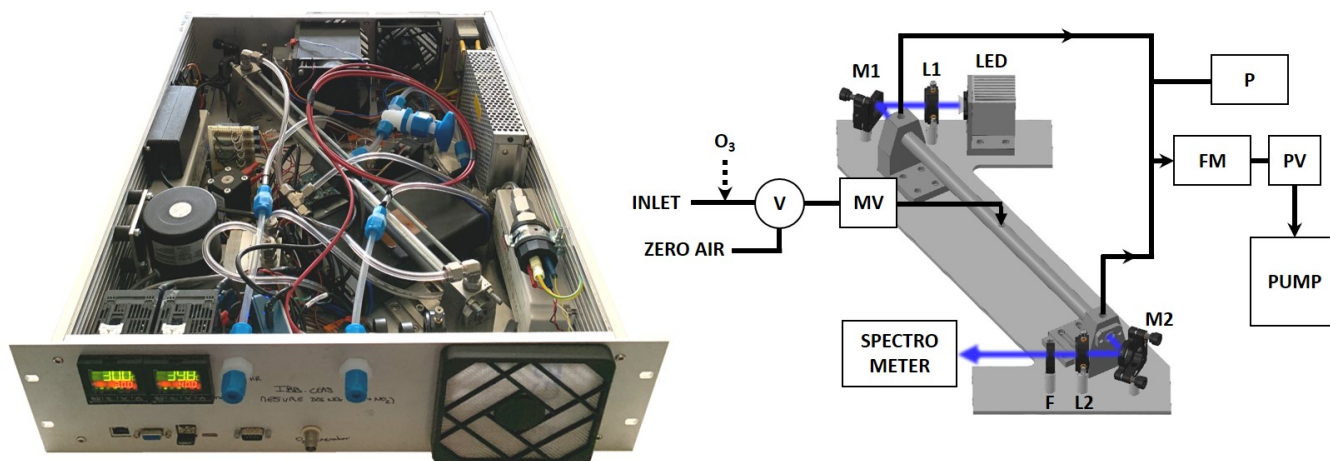
Figure 1. (left) A picture of the instrument mounted on a 19", 3U rack-mount case. (right) Schematic of the instrument. The LED is protected by a cap in which a photodiode (PD) is monitoring its power. The light from the LED is collimated by lens L1 and injected into the cavity. The exiting light is then collimated with lens L2, and injected into the spectrometer. M1 and M2 are steering mirrors and F is an optical filter. The gas line is composed of a pump, a pressure sensor P, a flow meter FM, and a proportional valve PV. At the inlet, a 3-way 2-position valve in PTFE, V, is used to switch between the sample and zero-air. A manual PFA needle valve MV, is used to fix the flow rate. An ozonizer can be inserted in the inlet line for NO_x measurements.

In IBBCEAS a broadband incoherent light source is coupled to a high-finesse optical cavity for trace gas detection. A picture of the spectrometer and a schematic diagram of the setup is shown in Figure 1. In the present study, the broadband light source consisted of a high-power LED Luminus SBT70 allowing ~ 1 W of optical power to be injected into the resonator. A thermoelectric (TEC) Peltier cooler (ET-161-12-08-E) and a fan / heatsink assembly were used to directly evacuate outside of the instrument up to ~ 75 W of thermal heat from the LED. A temperature regulator (RKC RF100) with a PT100 thermistor was used to stabilize the LED temperature at ± 0.1 °C. The LED spectrum was centered at 445 nm with 19 nm FWHM (Full Width at Half Maximum) which covers the main absorption features of NO_2, IO, CHOCHO and O_3. For better collimation of the LED spatially divergent emission (7 mm^2 surface), a dedicated optic (Ledil HEIDI RS) was used and coupled with a 25 mm focal lens (L1, Thorlabs, LA1951-A). The high-finesse optical cavity was formed by two half-inch diameter high reflectivity mirrors (maximum reflectivity at 450 nm $\geqslant 99.990 \pm 0.005$ %, Layertec, 109281) separated by a 41.7 cm-long PFA tube (14 mm internal diameter, 1 mm thick) hold by an external stainless-steel tube. Both mirrors were pre-aligned and glued with Torr Seal epoxy glue on removable stainless-steel supports which were then screwed on the cavity holders. This enables the easy cleaning

of the mirrors when required and also the removal of the cavity tube to perform open-cavity measurements, which is of interest for the detection of the highly reactive IO radical. Behind the cavity, a Thorlabs FB450-40 filter was used in order to remove the broadband component of the radiation sitting outside the highly reflective curve of the cavity mirrors. The radiation is focused on an optical fiber (FCRL-7UV100-2-SMA-FC) using a 40 mm focal lens (L2, Thorlabs, LA1422-A). The optical fiber input was composed of 7 cores in a round shape pattern on the collecting side, whereas, at the fiber end, on the spectrometer side, the cores were assembled in a line for better matching the 100 μm slit at the spectrometer. The spectrometer (Avantes, AvaSpec ULS2048L) was composed of a diffraction grating (2,400 lines mm^{-1}) and 2,048 pixels charge-coupled device (CCD). The resolution of the spectrometer was 0.54 ± 0.10 nm. All the optics including the cavity were mounted on a Z-shaped 8-mm thick aluminum board fixed on the rack using cylindrical dampers (Paulstra). On the board, four 5 W heating bands and one PT100 sensor were glued, and a second RKC module used to regulate its temperature. The board therefore acts as a large radiator inside the instrument, allowing to minimize internal thermal gradients and thermalize the instrument. Air circulation from outside is ensured by an aperture at the front and a fan placed at the back wall of the instrument (Figure 1). The gas line system was composed of a manual PFA needle valve (MV) and a 3-way 2-position PTFE valve, V (NResearch, 360T032) at the entrance ; while a proportional valve PV (Burkert, 239083), a flowmeter F (Honeywell, HAFUHT0010L4AXT), a pressure sensor P (STS ATM.ECO - accuracy ± 0.2 %) and a diaphragm pump (KNF, N 816 AV.12DC-B) were placed after the cavity. The entire line was made of ¼" PFA tubing which was found to be least lossy for the transport of highly reactive species (Grilli et al., 2012). The pump provided a constant flow that can reach 11 L min^{-1} at the end of the gas line while a constant pressure in the cavity was obtained by a PID regulator on the proportional valve. A data acquisition card (National Instruments, USB 6000) was interfaced to read the analogue signal from the pressure sensor, while a microcontroller (Arduino Due) drived the proportional valve. The manual valve at the entrance allowed to tune the flow rate. At the inlet, a 3-way 2-position PTFE valve allowed to switch between the gas sample and zero-air mixture for acquiring a reference spectra in the absence of absorption. Zero-air was produced by flowing outdoor air through a filtering system (TEKRAN, 90-25360-00 Analyzer Zero Air Filter). Particle filters (Whatman® PTFE membrane filters – TE 38, 5 μm, 47 mm) were also placed in the inlet lines (reference and sample) for preventing optical signal degradation due to Mie scattering as well as a degradation of the mirror reflectivity for long term deployment. The air flow was introduced at the center of the cavity and extracted at both ends of the cavity. The optimal cavity design was selected by running SolidWorks flow simulations at flow rates between 0.5 and 1 L min^{-1}. Cavity mirrors were positioned in order to maximize the sample length d, and to avoid localized turbulences in front of the mirrors (see supplementary informations SI - 1.1). The LED's power is monitored over time using a photodiode, PD, (Hamamatsu, S1223-01), allowing to discriminate if a decreasing of intensity at the CCD (during the acquisition of the spectra in absence of asborber) is due to a decreasing of the LED intensity or to the mirrors cleanliness degradation (for more details see SI - 1.2). All the components fit in a 19", 3U aluminum rack-mount case, have a total weight of 15 kg and a total electrical power consumption < 300 W. Instrument interface, measurements and data analysis are performed automatically, without the intervention of an operator, by dedicated LabView software. Instrument calibrations, however, must be performed by an operator on a regular basis.

3 Spectral fit

The absorption spectrum is calculated as the ratio between the spectrum of the light transmitted through the cavity without a sample, $I_0(\lambda)$, and with a sample in the cavity, $I(\lambda)$. It is expressed as the absorption coefficient (in units of cm^{-1}) by the following equation (Fiedler et al., 2003):

$$\alpha(\lambda) = \left(\frac{I_0(\lambda)}{I(\lambda)} - 1 \right) \left(\frac{1 - R(\lambda)}{d} \right) \tag{1}$$

where $R(\lambda)$ is the wavelength dependent mirror reflectivity and d the length of the sample inside the cavity. Equation (1) is derived from the Beer-Lambert's law and applied to light in an optical resonator (Ruth et al., 2014). The light transmitted through the optical cavity is attenuated by different processes such as absorption, reflection and scattering of the mirror sub-strates and coating, as well as losses due to the medium inside the cavity. The losses of the cavity mirrors are assumed to be constant between the acquisition of the reference and the sample spectrum. Mie scattering is minimized with a 5 μm particle filter in the gas inlet, while Rayleigh scattering losses were calculated to be 2.55×10^{-7} cm^{-1} at 445 nm at 25 °C and 1 atm (Kovalev and Eichinger, 2004) and thus negligible with respect to the cavity losses normalized by the cavity lengh ($\frac{1-R}{d} = 2.28 \times 10^{-6}$ cm^{-1}). Therefore, the light transmitted through the cavity is mainly affected by the absorption of the gas species, which leads to well-defined absorption spectral features, $\alpha_i(\lambda)$, that are analyzed in real time by a linear multicomponent fit routine. Experimental absorption spectra of the species i (i = NO_2, IO, CHOCHO and O_3) have been compared with literature cross section data accounted for the gas concentration, experimental conditions of temperature and pressure, and convoluted with the spectrometer instrumental function. Those experimental spectra are then used as reference spectra for the fit.

$$\alpha(\lambda) = \sum_i \sigma_i(\lambda) c_i + p(\lambda) \tag{2}$$

A fourth order polynomial function, $p(\lambda) = a_0 + a_1\lambda + a_2\lambda^2 + a_3\lambda^3 + a_4\lambda^4$, is added to the absorption coefficient equation (2) to adjust the spectral baseline and account for small changes between the reference and the sample spectra. The transmitted light intensity, as well as the optical absorption path, will be modulated by the shape of the mirror reflectivity curve. Therefore, the later should be defined in order to retrieve the correct absorption spectrum recorded at the cavity output.

4 Calibration, performance and multi-species detection

4.1 Calibration

Washenfelder et al. (2008) described a procedure for retrieving the mirror reflectivity curve by taking advantage of a different Rayleigh scattering contribution to the cavity losses while the measuring cell was filled with different bulk gases (e.g., helium versus air or nitrogen). The Rayleigh's empirical cross sections used by Min et al. (2016) and the theoretical ones used by Thalman and Volkamer (2010) were found to disagree, leading this work to propose an easier approach consisting of using trace gases at known concentrations (in this case NO_2 produced by a calibrator "Gas Standard Generator FlexStream™" from Kin-Tek Analytical, Inc. and CHOCHO produced by evaporating a glyoxal solution 40% in water from Sigma-Aldrich, since

O$_3$ spectrum is less structured and IO is highly reactive) and their literature cross-sections (Vandaele et al. (1998) for NO$_2$ and Volkamer et al. (2005) for CHOCHO) for retrieving the wavelength dependent reflectivity curve. Such an approach to calculate mirror reflectivity has been proposed before (Venables et al., 2006) and has been used by previous studies (Duan et al., 2018).

160 The shape of the reflectivity curve is adjusted to best match the convoluted literature NO$_2$ spectrum at the concentration given by the Kin-Tek calibrator (for more informations SI - 2). Figure 2(a) shows the resulting reflectivity curve and the transmitted light through the cavity and the optical filter. The maximum reflectivity achieved with both mirrors given by the calibration procedure is 99.9905 % leading to an effective optical path length of $\sim$ 4.4 km and a cavity finesse (F = $\frac{\pi\sqrt{R}}{(1-R)}$) of $\sim$ 33,100. While the shape of the mirror reflectivity curve is determined once and for all, its offset is slightly adjusted after each mirrors

165 cleaning, by flushing in the cavity a known concentration of NO$_2$. The spectral emission of the LED centered at 445 nm is well suited also for the detection of IO, CHOCHO and O$_3$, which are other key species in atmospheric chemistry. For the field measurements of NO$_2$ and NO$_x$, two twin instruments named IBBCEAS-NO$_2$ and IBBCEAS-NO$_x$ are deployed, with the later equipped with an ozone generator on the gas inlet line. At this wavelength region, water vapor also absorbs and is accounted for in the spectral fit analysis. However, the absorption of oxygen dimer is not required in the fit routine since the absorption

170 feature will be present in the reference (I_0) as well as in the an absorption (I) spectra. In Figure 2(b) simultaneous detection of NO$_2$, IO and O$_3$ is reported. Ozone, at 28.9 ppm, is produced by water electrolysis as described in Section 4.4, 191.8 ppb of NO$_2$ are provided by a permeation tube and 425.6 ppt of IO is generated by photochemical reaction of sublimated iodine crystals and ozone in the presence of radiation inside the cavity. For this spectrum, the light transmitted is integrated for 350 ms on the CCD and averaged over 1000 spectra, yielding to a 1σ standard deviation of the residuals of 4×10^{-8} cm^{-1} (Figure

175 2(b) bottom). In Figure 2(c) simultaneous detection of NO$_2$, CHOCHO and H$_2$O is reported. CHOCHO at 4.3 ppb is produced by evaporating a glyoxal solution (40% in water, Sigma-Aldrich) at the sample gas inlet of the instrument, NO$_2$ at 1.40 ppb and H$_2$O at 0.54 % are ambient concentrations observed in the laboratory during the experiment. For this spectrum, the light transmitted is integrated for 250 ms on the CCD and averaged over 1000 spectra, yielding to a 1σ standard deviation of the residuals of 5×10^{-9} cm^{-1} (Figure 2(c) bottom). The top Figure 2(b) and (c) show the experimental spectra (black traces), the

180 fit result (red traces) and contributions from each species(middle) which are included in the spectral fit. The concentrations of the species are retrieved with respect to the literature cross sections using the calibrated reflectivity curve discussed above
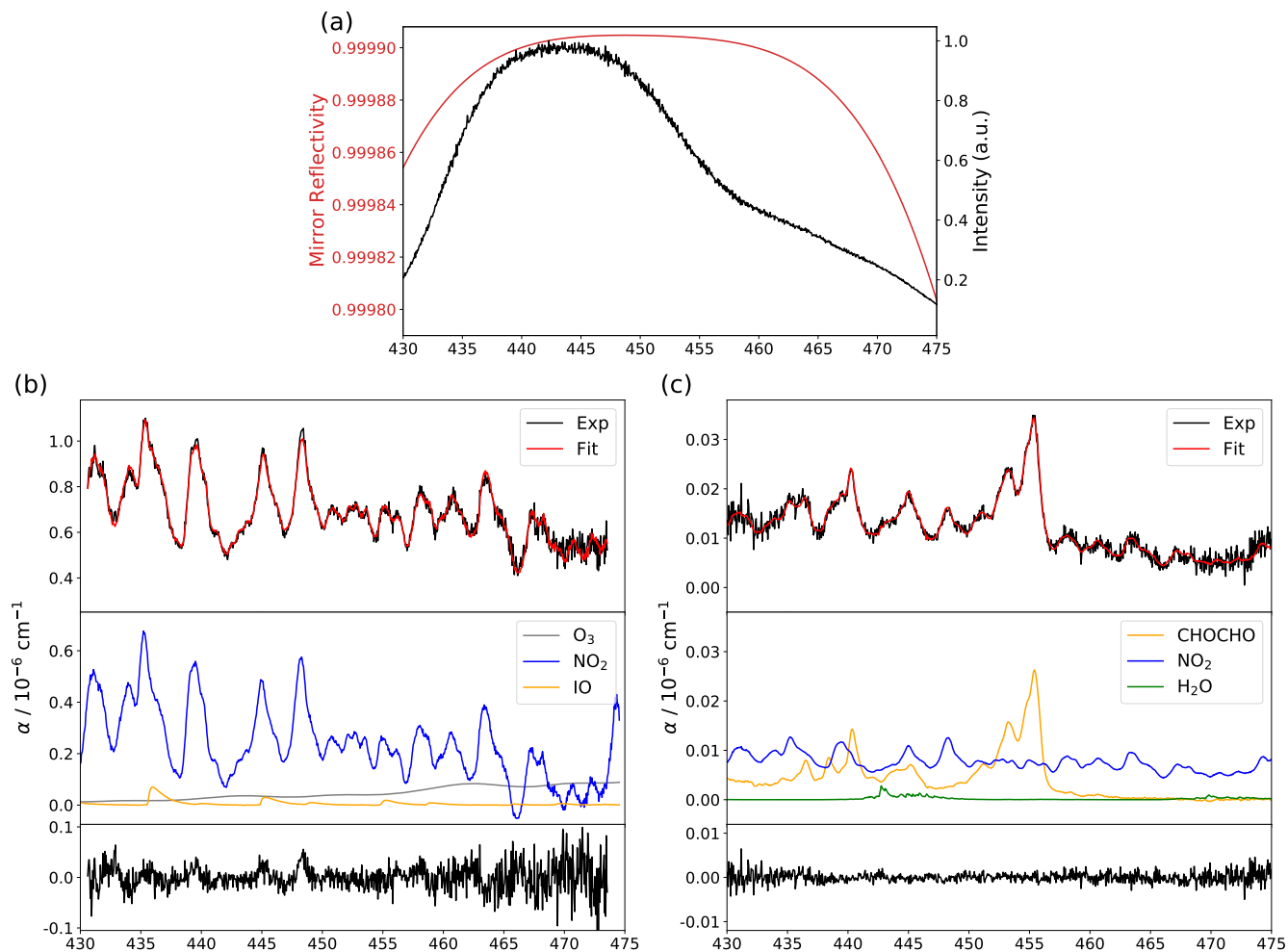
Figure 2. (a) The mirror reflectivity curve (red) in comparison with the spectrum of the LED light transmitted by the cavity and the optical filter for a single acquisition of 250 ms. (b) In black, an example of an experimental spectrum of NO_2, IO and O_3 at concentrations of 191.8 ppb, 425.6 ppt and 28.9 ppm, respectively ; in red, the multi-species spectral fit ; and in blue, orange and grey the absorptions of the different species. At the bottom (in black) the residual of the experimental fit with a 1σ standard deviation of 4×10^{-8} cm^{-1} after 1000 averages. (c) In black, an example of an experimental spectrum of NO_2, CHOCHO and H_2O at concentrations of 1.40 ppb, 4.3 ppb and 0.54 %, respectively ; in red, the multi-species spectral fit ; and in blue, orange and green the absorptions of the different species. At the bottom (in black) the residual of the experimental fit with a 1σ standard deviation of 5×10^{-9} cm^{-1} after 1000 averages.

4.2 Instrumental calibration and inter-comparison

A calibrator (Gas Standard Generator FlexStream™, Kin-Tek Analytical, Inc.) was used to produce a stable NO_2 source. The sample was produced using a permeation tube of NO_2 (Kin-Tek ELSRT2W) calibrated at an emission rate of 115 ng min^{-1} at 40 °C loaded into the calibrator. This type of calibrator is ideally suited for creating trace concentration mixtures (from ppt to ppm). The instruments were calibrated against the calibrator delivering NO_2 at 49.59 ± 0.17 ppb. To confirm the calibration process as well as the stability of the instrument within a greater range of concentrations, two inter-comparisons of the IBBCEAS with two different CLD instruments (ThermoFisher™, 42i NO_x analyser and ThermoFisher™, 42iTL NO_x trace analyser) were performed in outdoor air over 39 and 12 hours, respectively. Results are reported in Figure 3. The experiments took place at the Institute of Geosciences of the Environment (IGE) in Saint Martin d'Hères, France. The IGE is located in the university campus, $\sim$ 1 km from the city center of Grenoble and $\sim$ 300 m from a highway. Ambient air was pumped simultaneously from the same gas line by the instruments at flow rates of 1.0 and 0.5 L min^{-1} for the IBBCEAS and the CLD instrument (ThermoFisher™, 42i NO_x analyser), respectively. The measurements were conducted in September 2018. On Saturday 29th of September evening, the NO_2 peak occured at slightly later time than normally expected (from 8 pm to midnight), Figure 3(a). This may be due to the fact that during Saturday night, urban traffic can be significant until late, but also due to severe weather conditions prevailing at this time, with a storm and lightnings known to be a major natural source of NO_x (Atkinson, 2000). For the second experiment shown in Figure 3(b), ambient air was pumped at flow rates of 1.0 and 0.8 L min^{-1} for the IBBCEAS and the CLD trace instrument (ThermoFisher™, 42iTL NO_x trace analyser), respectively. The measurements were conducted in July 2019. Both instruments showed the expected variability of an urban environment with an increase of NO_2 in the evening and morning due to photochemical processes and anthropogenic activities (i.e mainly urban traffic).
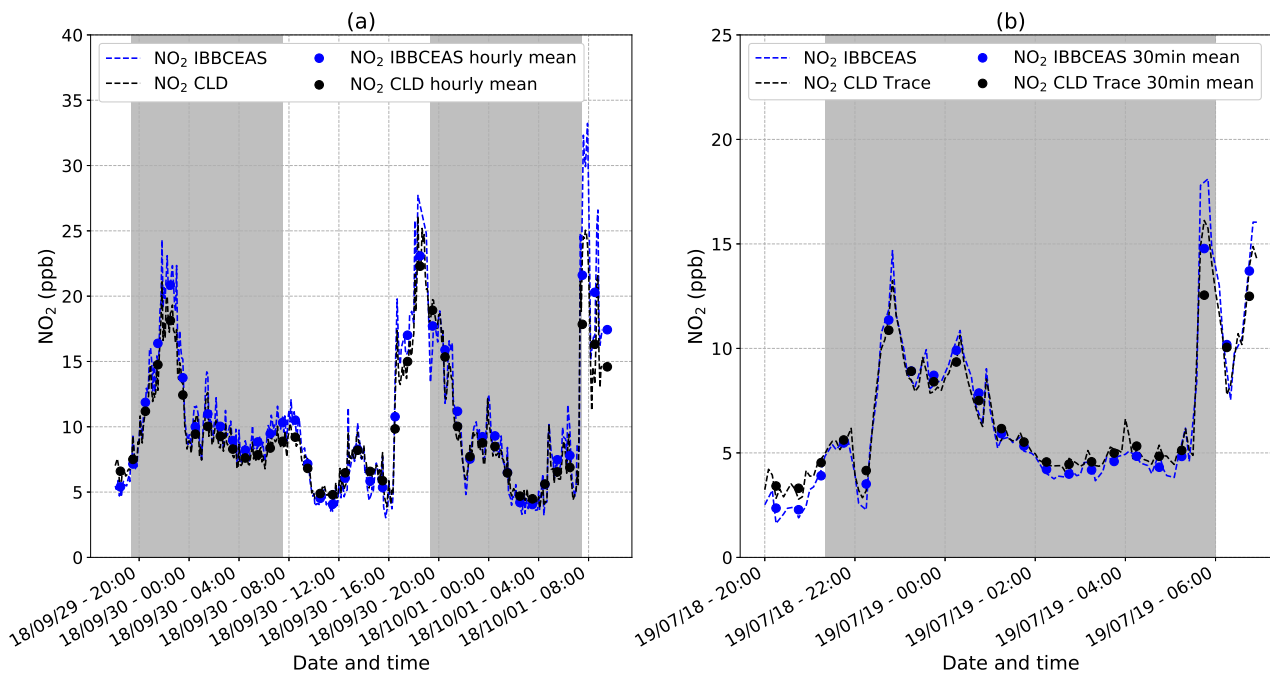
Figure 3. (a) A 39h-long intercomparison of the IBBCEAS instrument and the commercial CLD instrument (ThermoFischer™, 42i analyzer) on the NO$_2$ detection in outdoor urban area performed in September 2018. The plot reports continuous (dashed lines) and hourly (dots) average data for both techniques. The grey area corresponds to night time period. (b) A 12h-long intercomparison of the IBBCEAS instrument and the commercial CLD trace instrument (ThermoFischer™, 42iTL trace analyzer) on the NO$_2$ detection in outdoor urban area performed in July 2019. The plot reports continuous (dashed lines) and 30 minutes (dots) average data for both techniques. The grey area corresponds to night time period.

The correlation plot, based on data of all instruments, Figure 4(a), shows good linearity with a slope of 1.088 ± 0.005 and a correlation coefficient $R^2 = 0.989$ with measurements averaged over 5 minutes. In order to perform linearity tests, the previous NO$_2$ FlexStream™calibrator was used to produced various concentrations of NO$_2$ covering a large range of concentrations. Figure 4(b) shows the good linearity, from ppt to ppb range, of the IBBCEAS instrument with a slope of 1.015 ± 0.006 and a correlation factor of $R^2 = 0.9996$, confirming the validity of the calibration approach. The discrepancies observed between the IBBCEAS and the CLD techniques might be explained by positive and negative interferences on the CLD technique. While the system presented here measures NO$_2$ directly, the CLD technique applies an indirect measurement of NO$_x$ from the oxidation of NO through a catalyzer, then in CLD, the NO$_2$ mixing ratio is obtained by the subtraction of the NO signal to the total NO$_x$ signal. Villena et al. (2012), demonstrate that the interferences on a urban atmosphere for the CLD technique implied positive interferences when NO$_y$ species photolysis occurred, leading to an over-estimation of daytime NO$_2$ levels, while negative interferences were attributed to the VOCs photolysis followed by peroxyradical reactions with NO.
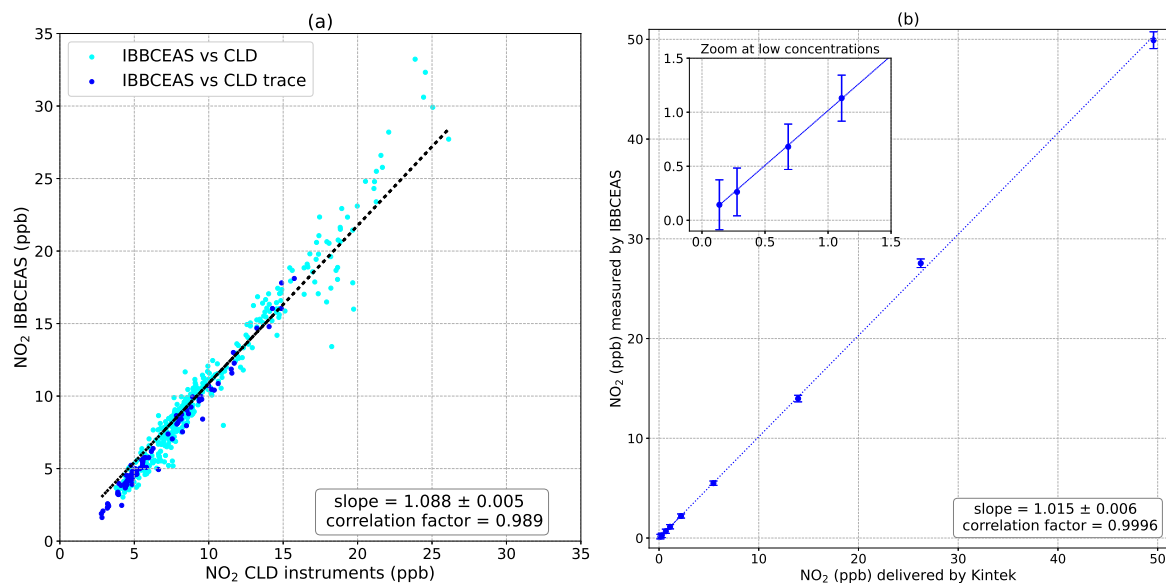
Figure 4. (a) A linear correlation was obtained with a slope of 1.088 $\pm$ 0.005 and a correlation coefficient $R^2 = 0.989$ between the IBBCEAS system and the ThermoFisher instruments. (b) Results of the system's calibration using a NO_2 FlexStream™calibrator. A linear correlation was obtained with a slope of 1.015 $\pm$ 0.005 and a correlation coefficient of $R^2 = 0.9996$

4.3 Performances

4.3.1 Instrument sensitivity and long-term stability

215 In remote area such as East Antarctica, NO_2 ranges from a few tens to a few hundreds of ppt (50 - 300 ppt) (Frey et al., 2013, 2015). Due to the low signal-to-noise ratio of the spectrometer, a single acquired spectrum (with an integration time ranging between 200 and 350 ms) does not provide the required detection limit. However, the sensitivity can be improved by averaging the measurements for longer times, over which the instrument is stable. The stability of the IBBCEAS system is mainly affected by temperature fluctuations, mechanical instabilities and pressure drifts. In order to characterize the long-term stability of the

220 instrument, two different studies were conducted on the IBBCEAS-NO_2 during the Antarctica field campaign at Dôme C in 2019-2020 (the same results for the IBBCEAS-NO_x can be found in the SI). For both studies, the light transmitted through the cavity (I) was integrated at the CCD for 250 ms, providing a signal-to-noise ratio of 110 for a single spectrum. The reference spectrum (I_0) was taken by averaging 2,000 individual spectra ($\sim$ 8 min) while flushing the cavity with zero-air. Subsequently, a 9h-long time series was recorded for each instrument maintaining the zero-air flow. The instrument was regulated at 12.0 $\pm$

225 0.2 °C, with a cavity pressure of 630.0 $\pm$ 0.7 mbar, and a gas flow of 1.02 $\pm$ 0.11 L min^{-1}. The minimum absorption coefficient (α_{min}), corresponding to the standard deviation of the residual of the spectrum, was deduced for different time averages. The results are shown in the log-log plot of Figure 5, were the dots are the data and the dashed line indicates the trend in case of pure white noise regime. From the graph one can see that the instrument follows the white noise trend for about 22 min (5,200

averages), afterwards, the baseline noise start to deviate due to the arise of frequency dependent noise. The choosen α_{min} value corresponds to 2.0×10^{-10} cm^{-1} within ~ 22 min (5,200 spectra) of measurement during wich a reference spectrum in absence of absorbers and the absorption spectrum are acquire. The corresponding figure of merit (Noise Equivalent Absorption Sensitivity, NEAS or $\alpha_{min(BW)} = \alpha_{min}$ x $\sqrt{\frac{t_{int}}{M}}$) is therefore 1.8×10^{-10} cm^{-1} Hz$^{-1/2}$ per spectral element (with t_{int} the integration time, ~ 11 min, and M the number of independent spectral elements, here 800 spectral elements are considered for the spectral fit).
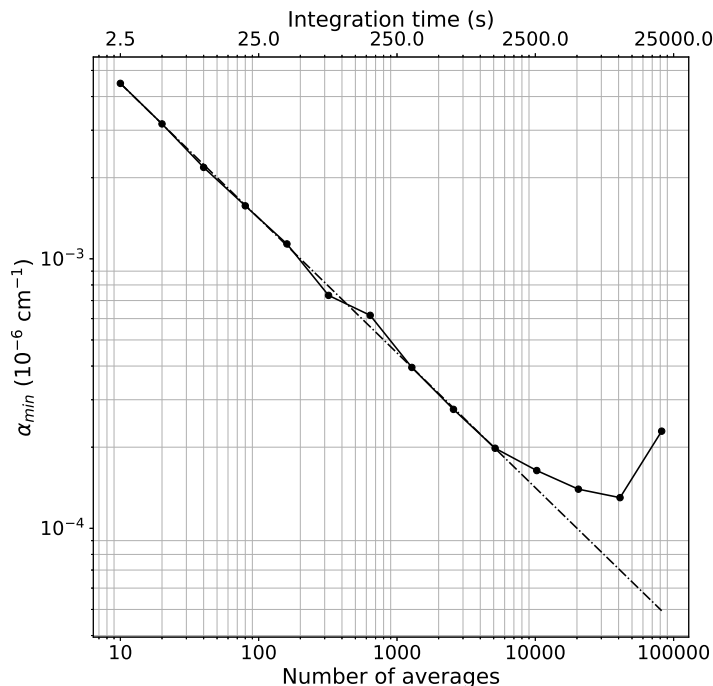
Figure 5. The minimum absorption coefficient α_{min} versus the number of spectral average for the IBBCEAS-NO$_2$ instrument. For these measurements the cell was continuously flushed with a flow of 1.02 L min^{-1} of zero-air, and the α_{min} was calculated from the standard deviation of the residual of the spectra at different time averages.

For the same time series, an Allan-Werle (AW) statistical method on the measured concentrations was employed (Werle et al., 1993). In this case, spectra were averaged in block of ten and analysed by the fit routine. The results of the fit are reported Figure 6 (left). For an acquisition time of 2.5 s, corresponding to 10 averaged spectra, the AW standard deviation $\sigma_{\mathrm{AW-SD}}$ was 175, 4.8, 125 ppt and 725 ppb for NO$_2$, IO , CHOCHO and O$_3$, respectively. By increasing the integration time, the $\sigma_{\mathrm{AW-SD}}$ decreased following the white noise trend, colored dashed line of Figure 6 (right), with a characteristic $\sqrt{N}$ slope (where N is the number of averaged spectra). Because a reference spectrum in absence of absorbents is required by this CEAS technique, depending on the shape of the AW plot, different strategies may be followed. In our case, the AW trends continue to decrease for all species during ~ 22 min (5,200 averages), this means that one can spend 11 minutes acquiring the reference spectrum
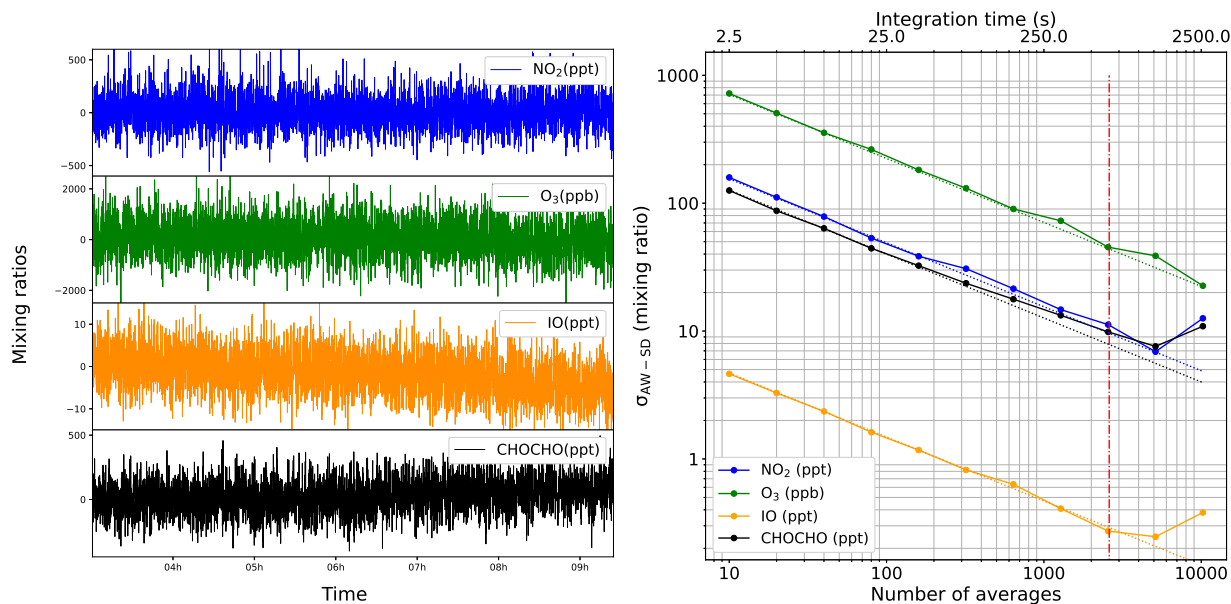
Figure 6. (left) Mixing ratios of the target species NO$_2$, O$_3$, IO, and CHOCHO, measured during a nine hours Allan-Werle variance statistical experiment flowing zero-air thought the cavity on the IBBCEAS-NO$_2$ instrument. (right) The log-log Allan-Werle standard deviation plot, illustrating that the instrument performance follows the white noise regime up to a certain extent, identified by the dashed lines. This represents the optimum integration time, after which instrumental instabilities start to dominate.

and further 11 minutes for the absorption spectrum, leading to limits of detection (LODs) of 11, 0.3, 10 ppt and 47 ppb (1σ) for NO$_2$, IO, CHOCHO and O$_3$, respectively. In our case, we chose to divide the measurement times by two (i.e $\sim$ 11 min and 2,600 averages for acquiring both the reference and the absorption spectra), offering equally interesting LODs: 16, 0.4, 12 ppt and 72 ppb for NO$_2$, IO, CHOCHO, and O$_3$ (1σ), respectively, and allowing us to stay within the white noise regime.
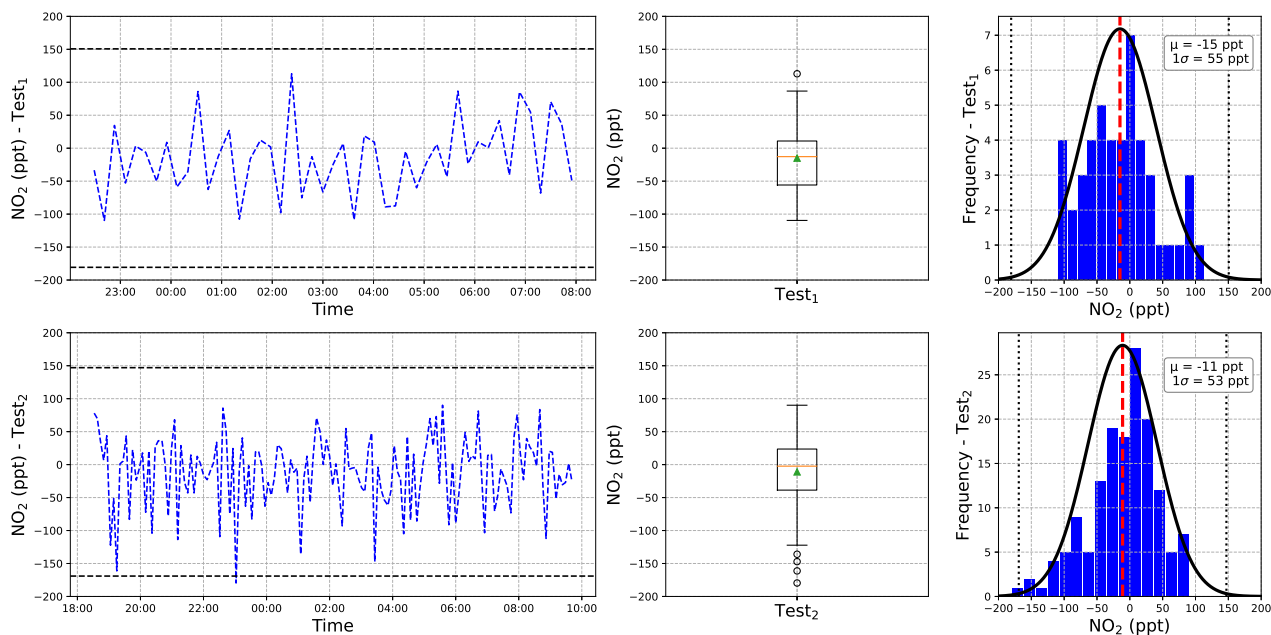
Figure 7. (left) timeseries of two long-term stability tests, the black dashed lines represent the 3σ ; (middle) boxplot of the stability test while continuously flushing zero-air in the cavity, means over 46 and 148 measurements (for Test$_1$ and Test$_2$, respectively), are shown as green triangles, dots represent the outliers ; (right) histogram analysis showing well distributed measurements within the 3σ (black dashed lines).

Long-term stability and repeatability of the instrument were further studied by taking regular reference spectra within the optimum integration time of the instrument while continuously flushing the instrument with zero-air mixture. In this case $\sim$ 5 min and $\sim$ 3 min intervals were chosen, corresponding to 1,024 and 580 averages (for 350 and 300 ms integration time, respectively) and a sensitivity on the NO$_2$ concentrations of 55 and 53 ppt (1σ), respectively. The results are reported in Figure 7. Test$_1$ (1,024 averages) was run for 9h and Test$_2$ (580 averages) for 15h. These tests highlight the reliability of the measurement protocol, with the long term measurement well distributed within the 3σ of the measurements precision (165 and 159 ppt, respectively). A Box-plot is also reported representing the average values (green triangles) and medians, quartiles, minimum and maximum values. The histogram analysis of those tests show a good distribution of the measurements within the 3σ.

Table 1 shows a comparison between the instrument presented in this work and other recently developed IBBCEAS systems. The detection limits are given in ppt min^{-1} (1σ) with the normalization time that accounts for the acquisition of the reference (without absorption) and sample spectra to allow a better comparison. It should be noticed that all the other developments took advantage from an optical spectrometer with a cooled CCD device to reduce dark noise. A more compact and affordable spectrometer was preferred in this work. The cooling at the CCD would allow to gain up to a factor of ten on the signal to noise ratio, which would directly apply to the achievable detection limits. Furthermore, a CCD with a higher sensitivity would allow

to select higher reflective mirrors and increase the optical pathlength. Noteworthy, the optimum integration time, corresponding to a minimum of the σ_{AW-SD}, is at 1,300 s ($\sim$ 22 min), allowing to achieve low detection limits even without a cooled CCD.

Table 1. Comparisons of the performances with other recently developed IBBCEAS systems

References	Centered wavelengh (nm)	Source FWHM (nm)	NO_2 detection limit (ppt min^{-1})	Sample path lengh (cm)	Mirror reflectivity (%)	Optical lengh (km)	Mirrors purged	CCD cooled (°C)	Minimum σ_{AW-SD} deviation (s)
Min et al. (2016)	455	18	16	48	99.9973	17.8	no	-70	100
Jordan et al. (2019)	505	30	200	102	99.98	5.1	yes	-80	300
Liu et al. (2019)	455	18	33	84	99.993	10.3	yes	-70	100
Liang et al. (2019)	448	15	15	58.9	99.9942	11.7	yes	-10	3,500
This work (2020)	450	19	40	41.7	99.9905	4.4	no	no	1,300

4.4 Indirect measurement of NO

Measuring NO and NO_2 simultaneously is important to study the NO_x budget in the atmosphere. In the selected blue visible region, there are no NO absorption features for direct optical measurements, and optical absorption detection of NO is typically done in the infrared region (Richard et al., 2018). However, its detection can be performed by indirectly measuring NO_2 after chemical conversion of NO to NO_2 in a controlled O_3 excess environment. This will lead to the measurement of NO_x, which, coupled by a simultaneous detection of NO_2 will provide the concentration of NO ([NO] = [NO_x] - [NO_2]) (Fuchs et al., 2009):

$$NO + O_3 \rightarrow NO_2 + O_2 \qquad \qquad k_1 = 1.80 \text{ x } 10^{-14} \text{ cm}^3 \text{ molec}^{-1} \text{ s}^{-1} \text{ at 25 °C} \qquad (R1)$$
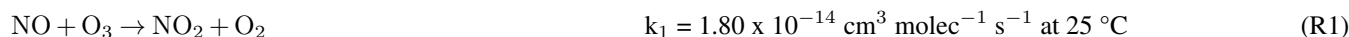
O_3 was produced by electrolysis of water using commercial ozone-micro-cells (INNOVATEC) allowing the generation of O_3 without nitrogen oxides impurities and without the need of an oxygen gas bottle. The cells were mounted in a home-made plastic container offering a 200 cm^3 water reservoir. With a miniaturized design (15 x 15 x 15 cm^3), ozone production can be controlled upon injection into the inlet line. The sample air flow to be analyzed works as carrier gas for flushing the ozone enriched surface water. This design also prevents the production of unwanted oxidizing agents such as peroxides, as well as sample dilution, causing a signal degradation and requiring precise flow measurements for quantitative analysis. The production of O_3 is controllable by the amount of electrolytic cells used and the supplied current, offering a dynamic range of 0 – 50 ppm of O_3 for a 1 L min^{-1} total flowrate. A diagram and details of the system can be found in the supplementary informations SI - 3.2. For long-term use of the instrument, the overall water consumption should be considered. Losses due to evaporation were estimated to be between 7 and 30 cm^3 per day at 10 and 30 °C respectively for a flow rate of 1 L min^{-1} while losses due to electrolysis are negligible, with only 0.024 cm^3 per day of consumption. The other parameter to consider is the mixing time between the ozone generator and the measurement cell with respect to the O_3 excess. For instance, the calculated production rate of NO_2 from (R1) (i.e. reaction speed or conversion rate of NO) is $v = 4.20 \times 10^{11}$ molecules cm^3 s^{-1} for 5 ppb of NO and 8 ppm of O_3. Under these conditions, a mixing time of 0.29 s is required for completing the conversion. With an air flow of 1 L min^{-1}, a 40-cm long 4-mm internal diameter tube is therefore required between the ozone generator and the measurement

cell. The performance of the ozone generation system was tested on the IBBCEAS instrument with a nitrogen oxide standard gas bottle containing ~ 195 ppb of NO in air (Air Liquide). Kinetic simulations using Tenua software (Wachsstock, 2007), were made in order to establish the O_3 excess concentrations needed to achieve the complete conversion of NO to NO_2, which, along with its detection, was tested with the IBBCEAS instrument by varying the excess concentration of O_3 until complete conversion of NO was achieved at different flows (i.e. different reaction times before reaching the measurement cell). The experimental results were in good agreement with the simulations as reported in Figure SI-9. In addition, the instrument was found to have a linear response regarding the detection of the produced O_3. The detection limit for the NO_x measurement was found to be similar to the one of NO_2, 10 ppt (1σ) in 22 min of integration time, while for NO, retrieved as the difference between the NO_x and the NO_2 concentrations, the detection limit estimated from the error propagation corresponds to 21 ppt.

5   Possible chemical and spectral interferences

Further possible interferences on NO_2 detection in the presence of high levels of O_3 were also studied, since a large excess of O_3 could trigger the following reactions with rate constants that are few orders of magnitude lower than k_1 (from the NIST Kinetics Database):

$$NO_2 + O_3 \rightarrow NO_3 + O_2 \qquad\qquad k_2 = 3.8 \text{ x } 10^{-17} \text{ cm}^3 \text{ molec}^{-1} \text{ s}^{-1} \text{ at } 25 \text{ °C} \qquad\qquad \text{(R2)}$$

$$NO_2 + O_3 \rightarrow 2O_2 + NO \qquad\qquad k_3 = 1.0 \text{ x } 10^{-18} \text{ cm}^3 \text{ molec}^{-1} \text{ s}^{-1} \text{ at } 25 \text{ °C} \qquad\qquad \text{(R3)}$$

$$NO_3 + O_3 \rightarrow 2O_2 + NO_2 \qquad\qquad k_4 = 1.0 \text{ x } 10^{-17} \text{ cm}^3 \text{ molec}^{-1} \text{ s}^{-1} \text{ at } 25 \text{ °C} \qquad\qquad \text{(R4)}$$
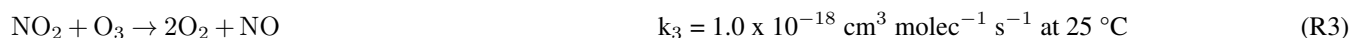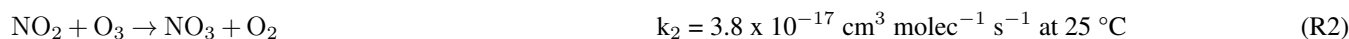
To study those possible interferences, 100 ppb of NO_2 produced by a permeation tube were pumped through the ozonizer and the spectrometer at a flow rate of 1 L min^{-1} while varying the concentration of O_3 from 0 to 10 ppm. NO_2 concentration was stable at low ozone concentrations, while a drop of 14 % was observed at high levels of O_3 ($\geqslant$ 8 ppm). Kinetics simulations showed that the NO_2 consumption in favor of the NO_3 production ($NO_2 + O_3 \rightarrow NO_3 + O_2$) was kinetically possible under those conditions. The consumption of NO_2 is strongly dependent on the reaction time and the concentration of O_3. The later should be selected according to the reaction time imposed by the volume of the inlet line and the flow rate, therefore making this interference negligible. Other chemicals reactions could led to an overestimation of NO_2 mixing ratios:

$$HONO \rightarrow NO + HO \qquad\qquad k_5 = 3.9 \text{ x } 10^{-21} \text{ cm}^3 \text{ molec}^{-1} \text{ s}^{-1} \text{ at } 25 \text{ °C} \qquad\qquad \text{(R5)}$$

$$HO_2NO_2 \rightarrow NO_2 + HO_2 \qquad\qquad k_6 = 1.3 \text{ x } 10^{-20} \text{ cm}^3 \text{ molec}^{-1} \text{ s}^{-1} \text{ at } 25 \text{ °C} \qquad\qquad \text{(R6)}$$
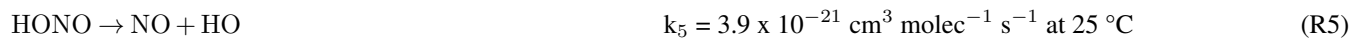
Couach et al. estimated the background levels of HONO and HO_2NO_2 in Grenoble to be 4 and 2 ppq (or 10^{-15} mol mol^{-1}), respectively (Couach et al., 2002). With such low concentrations and kinetic constant rates, interferences due to reactions (R5) and (R6) can be neglected in an urban envirintion. However, in remote areas such as the East Antarctic Plateau, HO_2NO_2 levels were estimated by indirect measurements to be around 25 ppt (Legrand et al., 2014). Because the lifetime of HO_2NO_2 decreases with temperature ($\tau_{HO_2NO_2}$ = 8.6 h at -30°C and 645 mbar), its measurement using an instrument stabilized at

higher temperature would lead to an overestimation of the NO_2 due to the thermal degradation of the HO_2NO_2. However, this interference can be minimized by working at low temperatures : at 10 °C and 1 L min^{-1} flow in our IBBCEAS instrument, the NO_2 signal would be overestimated by only 1 ppt, which is below the detection limit of the sensor. The instruments were therefore designed for working at low temperature (up to few degrees Celsius). One more reaction, (R7), may also lead to possible interferences on the NO_2 detection:

$$HONO + OH \rightarrow NO_2 + H_2O \qquad\qquad k_7 = 4.89 \text{ x } 10^{-12} \text{ cm}^3 \text{ molec}^{-1} \text{ s}^{-1} \text{ at 25 °C} \qquad\qquad \text{(R7)}$$
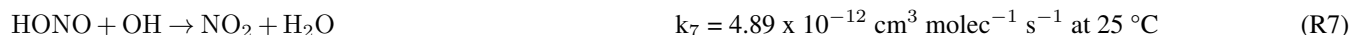
In urban environments OH radicals can be observed up to 4 x 10^6 OH radicals cm^{-3} (Heard, 2004; Mauldin et al., 2001). With background levels of HONO such as 4 ppq in the city of Grenoble and around 30 ppt in Dôme C, Antarctica (Legrand et al., 2014), very low mixing ratios of NO_2 (< few ppq) would be produced by (R7) in less than 8 s (residence time of the molecules in the instrument at 1 L min^{-1}). Therefore, contribution from this interference can be neglected. Previous works also highlighted possible artifacts through the heterogenous reaction of NO_2 and H_2O occurring in thin films on surfaces: the approximate rate production of HONO plus NO calculated in their study was reported to be between 4 x 10^{-2} and 8 x 10^{-2} ppb min^{-1} per ppm of NO_2 (Finlayson-Pitts et al., 2003). Assuming linearity between production rates and concentrations, this would represent a range of 8 to 16 ppq for 200 ppt of NO_2 in remote area such as the East Antarctic Plateau. The losses that may occur on the thin films on surfaces through the heterogeneous reaction of NO_2 and H_2O are therefore negligible. Finally, detection of NO_2, CHOCHO and IO may be affected by spectral interferences. For instance, water vapour also shows an absorption signature at this wavelength region which was included in the fit routine. Its spectral fit is important particularly for the measurement of NO_x, where the inlet sampling line gets saturated in water vapor while passing through the water reservoir of the ozone generator. In addition, artifacts on the signal and the spectral fit were studied by varying the O_3, NO_2 or NO mixing ratios in cavity. Small imperfections of the fit could lead to large effects on the NO_2 retrieved mixing ratio, particularly at sub-ppb concentrations and in presence of large amounts of ozone. However, no appreciable effects of possible artifacts were observed while O_3 concentrations up to 8 ppm were used. These performance studies and the simplicity of the ozone generator, compact and fully controllable, make it suitable for field applications.

6 Conclusions

A compact, robust, affordable and highly sensitive IBBCEAS instrument for direct detection of NO_2, IO, CHOCHO and O_3 and indirect detection of NO is reported in this work. The instrument relies on the injection of incoherent radiation from a compact, high power and low cost LED source, into a high-finesse optical cavity. The instrument provides a minimum detectable absorption of 2.0×10^{-10} cm^{-1} corresponding to a figure of merit (Noise Equivalent Absorption Sensitivity, NEAS) of 1.8×10^{-10} cm^{-1} Hz$^{-1/2}$ per spectral element. Due to the multiplexing broadband feature of the setup, multi-species detection can be performed with simultaneous detection of NO_2, IO, CHOCHO, and O_3 achieving detection limits of 11, 0.3, 10 ppt and 47 ppb (1σ) within 22 min of measurement (which account for the reference and absorption spectra acquisition), respectively. Detection limits for the indirect measurement of NO_x and NO are 10 and 21 ppt (1σ), respectively. The instrument

has been designed to fit in a 19", 3U rack-mount case, weights 15 kg and has a total electrical power consumption < 300 W.
The detection limits could be further improved by replacing the ULS2048L Avantes spectrometer, which offers at this working
wavelength a signal to noise ratio on a single acquisition of 110 and a sensitivity of 172,000 counts μW^{-1} ms^{-1}, with a
spectrometer with an integrated cooled CCD. The cooling would allow to gain up to a factor of ten on the signal to noise ratio,
which would directly apply to the detection limits. Better sensitivity of the CCD would also allow the use of higher reflectivity
mirrors as done by Min et al. (2016), providing an effective optical path length of $\sim$ 18 km (with similar cavity length), $\sim$ 4
times higher than the one obtained in this work. The dynamic ranges, detection limits and multi-species detection character
make this instrument well suitable for measurements in different environments, from highly polluted to very remote areas such
as polar regions. The instruments can be used in the future to address different scientific questions, related to the oxidative
capacity at particular regions (i.e. inland and coastal polar atmospheres), where variability of NO_x and IO would provide key
information for understanding the mechanisms taking place in such remote areas. The detection of the α-dicarbonyl CHOCHO
may have applications at the marine boundary layer, where its source remains unknown and its contribution to secondary
aerosol particle formation may be relevant (Ervens et al., 2011; Volkamer et al., 2007; Fu et al., 2008).

Data availability. Available on request

Author contributions. Grants obtained by JS, AD and RG funded the project. The IBBCEAS instruments were designed and developed by
CB under the supervision of RG. AB developed and validated the ozone generation. The instruments were optimized and validated by CB
and AB who also did the instrumental intercomparison, the measurements for the long-term stability and the simulations and study of the
possible chemical interferences. RG was the principal supervisor of the project. JS and AD contributed with their knowledges in atmospheric
sciences and they closely followed the project with regular meetings. JS and RG are the supervisors of AB PhD thesis under which the
instruments are deployed. NC provided technical and engineering inputs particularly at the beginning of the project. The manuscript was
written by AB, CB and RG, with all authors contributions.

Competing interests. no competing interests are present

Acknowledgements. The research leading to these results has received funding from: PARCS project (Pollution in the ARCtic System,
a project of the CNRS French Artic Initiative: http://www.chantier-arctique.fr/en) ; the LabEx OSUG@2020 ("Investissements d'avenir"
– ANR10 LABX56) ; the French National program LEFE (Les Enveloppes Fluides et l'Environnement) ; the Agence Nationale de la
Recherche (ANR) via contract ANR-16-CE01-0011-01 EAIIST ; the Foundation BNP-Paribas through its Climate initiative program and by
the French Polar Institute (IPEV) through programs 1177 (CAPOXI 35–75) and 1169 (EAIIST). The authors would like to thank the LabEx
OSUG@2020 for funding the ThermoFisher™, 42i NO_x analyzer and IPEV for funding the ThermoFisher 42iTL™, NO_x trace analyzer that

were used during the development of the IBBCEAS instruments presented here. The authors thank G. Méjean and D. Romanini from LIPhy, France, for the very useful exchange of informations on IBBCEAS technique as well as A. A. Ruth from the University of Cork, Ireland, for his very useful feedbacks on the manuscript. And finally, the authors greatly thank the technical staff of the IGE for their technical support.

385 The authors thank S. Houdier for the discussions about the Glyoxal measurement.

References

Atkinson, D. B.: Solving chemical problems of environmental importance using Cavity Ring-Down Spectroscopy, The Analyst, 128, 117–125, https://doi.org/10.1039/b206699h, http://xlink.rsc.org/?DOI=b206699h, 2003.

Atkinson, R.: Atmospheric chemistry of VOCs and NOV, Atmospheric Environment, p. 39, 2000.

Brown, S. S., Stark, H., Ciciora, S. J., McLaughlin, R. J., and Ravishankara, A. R.: Simultaneous in situ detection of atmospheric NO_3 and N_2O_5 via Cavity Ring-Down Spectroscopy, Review of Scientific Instruments, 73, 3291–3301, https://doi.org/10.1063/1.1499214, http://aip.scitation.org/doi/10.1063/1.1499214, 2002.

Chan, K. L., Pöhler, D., Kuhlmann, G., Hartl, A., Platt, U., and Wenig, M. O.: NO_2 measurements in Hong Kong using LED based Long Path Differential Optical Absorption Spectroscopy, Atmospheric Measurement Techniques, 5, 901–912, https://doi.org/10.5194/amt-5-901-2012, https://www.atmos-meas-tech.net/5/901/2012/, 2012.

Couach, O., BALlN, J., Jimenez, R., Rjstorj, P., Simeonov, V., QUAGLlA, P., and Clappier, A.: Etude d'un épisode photochimique à l'alde d'un modèle méso-échelle et de mesures intensives sur la région de Grenoble - Study of a photochemical episode over the Grenoble area using a mesoscale model and intensive measurements, p. 19, 2002.

Dooly, G., Fitzpatrick, C., and Lewis, E.: Deep UV based DOAS system for the monitoring of nitric oxide using ratiometric separation techniques, Sensors and Actuators B: Chemical, 134, 317–323, https://doi.org/10.1016/j.snb.2008.05.011, https://linkinghub.elsevier.com/retrieve/pii/S0925400508003316, 2008.

Duan, J., Qin, M., Ouyang, B., Fang, W., Li, X., Lu, K., Tang, K., Liang, S., Meng, F., Hu, Z., Xie, P., Liu, W., and Häsler, R.: Development of an Incoherent BroadBand Cavity-Enhanced Absorption Spectrometer for in situ measurements of HONO and NO_2, Atmospheric Measurement Techniques, 11, 4531–4543, https://doi.org/10.5194/amt-11-4531-2018, https://www.atmos-meas-tech.net/11/4531/2018/, 2018.

Ervens, B., Turpin, B. J., and Weber, R. J.: Secondary organic aerosol formation in cloud droplets and aqueous particles (aqSOA): a review of laboratory, field and model studies, Atmospheric Chemistry and Physics, 11, 11 069–11 102, https://doi.org/10.5194/acp-11-11069-2011, https://www.atmos-chem-phys.net/11/11069/2011/, 2011.

Fiedler, S. E., Hese, A., and Ruth, A. A.: Incoherent Broad-Band Cavity-Enhanced Absorption Spectroscopy, Chemical Physics Letters, 371, 284–294, https://doi.org/10.1016/S0009-2614(03)00263-X, https://linkinghub.elsevier.com/retrieve/pii/S000926140300263X, 2003.

Finlayson-Pitts, B. J. and Pitts, J. N.: CHAPTER 4 - Photochemistry of important atmospheric species, in: Chemistry of the Upper and Lower Atmosphere, edited by Finlayson-Pitts, B. J. and Pitts, J. N., pp. 86 – 129, Academic Press, San Diego, https://doi.org/10.1016/B978-012257060-5/50006-X, http://www.sciencedirect.com/science/article/pii/B978012257060550006X, 2000.

Finlayson-Pitts, B. J., Wingen, L. M., Sumner, A. L., Syomin, D., and Ramazan, K. A.: The heterogeneous hydrolysis of NO_2 in laboratory systems and in outdoor and indoor atmospheres: an integrated mechanism, Physical Chemistry Chemical Physics, 5, 223–242, https://doi.org/10.1039/b208564j, http://xlink.rsc.org/?DOI=b208564j, 2003.

Frey, M. M., Brough, N., France, J. L., Anderson, P. S., Traulle, O., King, M. D., Jones, A. E., Wolff, E. W., and Savarino, J.: The diurnal variability of atmospheric nitrogen oxides (NO and NO_2) above the antarctic plateau driven by atmospheric stability and snow emissions, Atmospheric Chemistry and Physics, 13, 3045–3062, https://doi.org/10.5194/acp-13-3045-2013, https://www.atmos-chem-phys.net/13/3045/2013/, 2013.

Frey, M. M., Roscoe, H. K., Kukui, A., Savarino, J., France, J. L., King, M. D., Legrand, M., and Preunkert, S.: Atmospheric nitrogen oxides (NO and NO_2) at Dome C, East Antarctica, during the OPALE campaign, Atmospheric Chemistry and Physics, 15, 7859–7875, https://doi.org/10.5194/acp-15-7859-2015, https://www.atmos-chem-phys.net/15/7859/2015/, 2015.

Fu, T.-M., Jacob, D. J., Wittrock, F., Burrows, J. P., Vrekoussis, M., and Henze, D. K.: Global budgets of atmospheric glyoxal and methylglyoxal, and implications for formation of secondary organic aerosols, Journal of Geophysical Research, 113, D15 303, https://doi.org/10.1029/2007JD009505, http://doi.wiley.com/10.1029/2007JD009505, 2008.

Fuchs, H., Dubé, W. P., Lerner, B. M., Wagner, N. L., Williams, E. J., and Brown, S. S.: A sensitive and versatile detector for atmospheric NO_2 and NO_x based on blue diode laser Cavity Ring-Down Spectroscopy, Environmental Science & Technology, 43, 7831–7836, https://doi.org/10.1021/es902067h, https://pubs.acs.org/doi/10.1021/es902067h, 2009.

Fuchs, H., Ball, S. M., Bohn, B., Brauers, T., Cohen, R. C., Heitmann, U., Jones, R. L., Kleffmann, J., Mentel, T. F., Kiendler-Scharr, A., Schlosser, E., Shillings, A. J. L., Tillmann, R., Varma, R. M., Venables, D. S., Tapia, G. V., Wahner, A., Wegener, R., Wooldridge, P. J., and Brown, S. S.: Intercomparison of measurements of NO_2 concentrations in the atmosphere simulation chamber SAPHIR during the NO_3Comp campaign, Atmos. Meas. Tech., p. 17, 2010.

Gherman, T., Venables, D. S., Vaughan, S., Orphal, J., and Ruth, A. A.: Incoherent Broadband Cavity-Enhanced Absorption Spectroscopy in the near-Ultraviolet: application to HONO and NO_2, Environmental Science & Technology, 42, 890–895, https://doi.org/10.1021/es0716913, https://pubs.acs.org/doi/10.1021/es0716913, 2008.

Grilli, R., Méjean, G., Kassi, S., Ventrillard, I., Abd-Alrahman, C., Fasci, E., and Romanini, D.: Trace measurement of BrO at the ppt level by a transportable Mode-Locked Frequency-Doubled Cavity-Enhanced Spectrometer, Applied Physics B, 107, 205–212, https://doi.org/10.1007/s00340-011-4812-9, http://link.springer.com/10.1007/s00340-011-4812-9, 2012.

Grosjean, D. and Harrison, J.: Response of chemiluminescence NO_x analyzers and ultraviolet ozone analyzers to organic air pollutants, Environmental Science & Technology, 19, 862–865, https://doi.org/10.1021/es00139a016, https://pubs.acs.org/doi/abs/10.1021/es00139a016, 1985.

Heard, D. E.: High levels of the hydroxyl radical in the winter urban troposphere, Geophysical Research Letters, 31, L18 112, https://doi.org/10.1029/2004GL020544, http://doi.wiley.com/10.1029/2004GL020544, 2004.

Jaworski, N. A., Howarth, R. W., and Hetling, L. J.: Atmospheric deposition of nitrogen oxides onto the landscape contributes to coastal eutrophication in the northeast United States, Environmental Science & Technology, 31, 1995–2004, https://doi.org/10.1021/es960803f, https://pubs.acs.org/doi/10.1021/es960803f, 1997.

Jordan, N., Ye, C. Z., Ghosh, S., Washenfelder, R. A., Brown, S. S., and Osthoff, H. D.: A Broadband Cavity-Enhanced Spectrometer for atmospheric trace gas measurements and Rayleigh scattering cross sections in the cyan region (470–540 nm), Atmospheric Measurement Techniques, 12, 1277–1293, https://doi.org/10.5194/amt-12-1277-2019, https://www.atmos-meas-tech.net/12/1277/2019/, 2019.

Kovalev, V. A. and Eichinger, W. E.: Elastic Lidar: theory, practice, and analysis methods, John Wiley & Sons, Inc., Hoboken, NJ, USA, https://doi.org/10.1002/0471643173, http://doi.wiley.com/10.1002/0471643173, 2004.

Langridge, J. M., Ball, S. M., and Jones, R. L.: A compact Broadband Cavity Enhanced Absorption Spectrometer for detection of atmospheric NO_2 using light emitting diodes, The Analyst, 131, 916, https://doi.org/10.1039/b605636a, http://xlink.rsc.org/?DOI=b605636a, 2006.

Lee, J., Kim, K.-H., Kim, Y. J., and Lee, J.: Application of a Long-Path Differential Optical Absorption Spectrometer (LP-DOAS) on the measurements of NO_2, SO_2, O_3, and HNO_2 in Gwangju, Korea, Journal of Environmental Management, 86, 750–759, https://doi.org/10.1016/j.jenvman.2006.12.044, https://linkinghub.elsevier.com/retrieve/pii/S0301479707000102, 2008.

Lee, J. S., Kim, Y. J., Kuk, B., Geyer, A., and Platt, U.: Simultaneous measurements of atmospheric pollutants and visibility with a Long-Path DOAS System in urban areas, Environmental Monitoring and Assessment, 104, 281–293, https://doi.org/10.1007/s10661-005-1616-6, http://link.springer.com/10.1007/s10661-005-1616-6, 2005.

Legrand, M., Preunkert, S., Frey, M., Bartels-Rausch, T., Kukui, A., King, M. D., Savarino, J., Kerbrat, M., and Jourdain, B.: Large mixing ratios of atmospheric nitrous acid (HONO) at Concordia (east antarctic plateau) in summer: a strong source from surface snow?, Atmospheric Chemistry and Physics, 14, 9963–9976, https://doi.org/10.5194/acp-14-9963-2014, https://www.atmos-chem-phys.net/14/9963/2014/, 2014.

Leser, H., Hönninger, G., and Platt, U.: MAX-DOAS measurements of BrO and NO_2 in the marine boundary layer, Geophysical Research Letters, 30, n/a–n/a, https://doi.org/10.1029/2002GL015811, http://doi.wiley.com/10.1029/2002GL015811, 2003.

Liang, S., Qin, M., Xie, P., Duan, J., Fang, W., He, Y., Xu, J., Liu, J., Li, X., Tang, K., Meng, F., Ye, K., Liu, J., and Liu, W.: Development of an Incoherent Broadband Cavity-Enhanced Absorption Spectrometer for measurements of ambient glyoxal and NO_2 in a polluted urban environment, Atmospheric Measurement Techniques, 12, 2499–2512, https://doi.org/10.5194/amt-12-2499-2019, https://www.atmos-meas-tech.net/12/2499/2019/, 2019.

Liu, J., Li, X., Yang, Y., Wang, H., Wu, Y., Lu, X., Chen, M., Hu, J., Fan, X., Zeng, L., and Zhang, Y.: An IBBCEAS system for atmospheric measurements of glyoxal and methylglyoxal in the presence of high NO_2 concentrations, Atmospheric Measurement Techniques, 12, 4439–4453, https://doi.org/10.5194/amt-12-4439-2019, https://www.atmos-meas-tech.net/12/4439/2019/, 2019.

Maeda, Y., Aoki, K., and Munemori, M.: Chemiluminescence method for the determination of nitrogen dioxide, Analytical Chemistry, 52, 307–311, https://doi.org/10.1021/ac50052a022, https://pubs.acs.org/doi/abs/10.1021/ac50052a022, 1980.

Mauldin, R. L., Eisele, F. L., Tanner, D. J., Kosciuch, E., Shetter, R., Lefer, B., Hall, S. R., Nowak, J. B., Buhr, M., Chen, G., Wang, P., and Davis, D.: Measurements of OH, H_2SO_4, and MSA at the South Pole during ISCAT, Geophysical Research Letters, 28, 3629–3632, https://doi.org/10.1029/2000GL012711, http://doi.wiley.com/10.1029/2000GL012711, 2001.

Min, K.-E., Washenfelder, R. A., Dubé, W. P., Langford, A. O., Edwards, P. M., Zarzana, K. J., Stutz, J., Lu, K., Rohrer, F., Zhang, Y., and Brown, S. S.: A Broadband Cavity Enhanced Absorption Spectrometer for aircraft measurements of glyoxal, methylglyoxal, nitrous acid, nitrogen dioxide, and water vapor, Atmospheric Measurement Techniques, 9, 423–440, https://doi.org/10.5194/amt-9-423-2016, https://www.atmos-meas-tech.net/9/423/2016/, 2016.

Monks, P., Granier, C., Fuzzi, S., Stohl, A., Williams, M., Akimoto, H., Amann, M., Baklanov, A., Baltensperger, U., Bey, I., Blake, N., Blake, R., Carslaw, K., Cooper, O., Dentener, F., Fowler, D., Fragkou, E., Frost, G., Generoso, S., Ginoux, P., Grewe, V., Guenther, A., Hansson, H., Henne, S., Hjorth, J., Hofzumahaus, A., Huntrieser, H., Isaksen, I., Jenkin, M., Kaiser, J., Kanakidou, M., Klimont, Z., Kulmala, M., Laj, P., Lawrence, M., Lee, J., Liousse, C., Maione, M., McFiggans, G., Metzger, A., Mieville, A., Moussiopoulos, N., Orlando, J., O'Dowd, C., Palmer, P., Parrish, D., Petzold, A., Platt, U., Pöschl, U., Prévôt, A., Reeves, C., Reimann, S., Rudich, Y., Sellegri, K., Steinbrecher, R., Simpson, D., ten Brink, H., Theloke, J., van der Werf, G., Vautard, R., Vestreng, V., Vlachokostas, C., and von Glasow, R.: Atmospheric composition change – global and regional air quality, Atmospheric Environment, 43, 5268–5350, https://doi.org/10.1016/j.atmosenv.2009.08.021, https://linkinghub.elsevier.com/retrieve/pii/S1352231009007109, 2009.

Monks, P. S.: Gas-phase radical chemistry in the troposphere, Chemical Society Reviews, 34, 376, https://doi.org/10.1039/b307982c, http://xlink.rsc.org/?DOI=b307982c, 2005.

Pikelnaya, O., Hurlock, S. C., Trick, S., and Stutz, J.: Intercomparison of MultiAXis and Long-Path Differential Optical Absorption Spectroscopy measurements in the marine boundary layer, Journal of Geophysical Research: Atmospheres, 112, https://doi.org/10.1029/2006JD007727, http://doi.wiley.com/10.1029/2006JD007727, 2007.

Platt, U. and Perner, D.: Direct measurements of atmospheric CH_2O, HNO_2, O_3, NO_2, and SO_2 by Differential Optical Absorption in the near UV, Journal of Geophysical Research: Oceans, 85, 7453–7458, https://doi.org/10.1029/JC085iC12p07453, http://doi.wiley.com/10.1029/JC085iC12p07453, 1980.

Pöhler, D., Vogel, L., Friess, U., and Platt, U.: Observation of halogen species in the Amundsen Gulf, Arctic, by active Long-Path Differential Optical Absorption Spectroscopy, Proceedings of the National Academy of Sciences, 107, 6582–6587, https://doi.org/10.1073/pnas.0912231107, http://www.pnas.org/cgi/doi/10.1073/pnas.0912231107, 2010.

Richard, L., Romanini, D., and Ventrillard, I.: Nitric oxide analysis down to ppt levels by Optical-Feedback Cavity-Enhanced Absorption Spectroscopy, Sensors, 18, 1997, https://doi.org/10.3390/s18071997, http://www.mdpi.com/1424-8220/18/7/1997, 2018.

Rozanov, V. V. and Rozanov, A. V.: Differential Optical Absorption Spectroscopy (DOAS) and air mass factor concept for a multiply scattering vertically inhomogeneous medium: theoretical consideration, Atmospheric Measurement Techniques, 3, 751–780, https://doi.org/10.5194/amt-3-751-2010, https://www.atmos-meas-tech.net/3/751/2010/, 2010.

Ruth, A. A., Dixneuf, S., and Raghunandan, R.: Broadband Cavity-Enhanced Absorption Spectroscopy with Incoherent Light, in: Cavity-Enhanced Spectroscopy and Sensing, edited by Gagliardi, G. and Loock, H.-P., vol. 179, pp. 485–517, Springer Berlin Heidelberg, Berlin, Heidelberg, https://doi.org/10.1007/978-3-642-40003-2_14, http://link.springer.com/10.1007/978-3-642-40003-2_14, 2014.

Ryerson, T. B., Williams, E. J., and Fehsenfeld, F. C.: An efficient photolysis system for fast-response NO_2 measurements, Journal of Geophysical Research: Atmospheres, 105, 26 447–26 461, https://doi.org/10.1029/2000JD900389, http://doi.wiley.com/10.1029/2000JD900389, 2000.

Sinreich, R., Volkamer, R., Filsinger, F., Friess, U., Kern, C., Platt, U., Sebastian, O., and Wagner, T.: MAX-DOAS detection of glyoxal during ICARTT 2004, Atmos. Chem. Phys., p. 11, 2004.

Thalman, R. and Volkamer, R.: Inherent calibration of a blue LED-CE-DOAS instrument to measure iodine oxide, glyoxal, methyl glyoxal, nitrogen dioxide, water vapour and aerosol extinction in open cavity mode, Atmospheric Measurement Techniques, 3, 1797–1814, https://doi.org/10.5194/amt-3-1797-2010, https://www.atmos-meas-tech.net/3/1797/2010/, 2010.

Triki, M., Cermak, P., Méjean, G., and Romanini, D.: Cavity-Enhanced Absorption Spectroscopy with a red LED source for NO_x trace analysis, Applied Physics B, 91, 195–201, https://doi.org/10.1007/s00340-008-2958-x, http://link.springer.com/10.1007/s00340-008-2958-x, 2008.

Vandaele, A., Hermans, C., Simon, P., Carleer, M., Colin, R., Fally, S., Mérienne, M., Jenouvrier, A., and Coquart, B.: Measurements of the NO_2 absorption cross-section from $42\,000\,cm^{-1}$ to $10\,000\,cm^{-1}$ (238–1000 nm) at 220 K and 294 K, Journal of Quantitative Spectroscopy and Radiative Transfer, 59, 171–184, https://doi.org/10.1016/S0022-4073(97)00168-4, https://linkinghub.elsevier.com/retrieve/pii/S0022407397001684, 1998.

Venables, D. S., Gherman, T., Orphal, J., Wenger, J. C., and Ruth, A. A.: High sensitivity in situ monitoring of NO_3 in an atmospheric simulation chamber using Incoherent Broadband Cavity-Enhanced Absorption Spectroscopy, Environmental Science & Technology, 40, 6758–6763, https://doi.org/10.1021/es061076j, https://pubs.acs.org/doi/10.1021/es061076j, 2006.

Ventrillard-Courtillot, I., Sciamma O'Brien, E., Kassi, S., Méjean, G., and Romanini, D.: Incoherent Broad-Band Cavity-Enhanced Absorption Spectroscopy for simultaneous trace measurements of NO_2 and NO_3 with a LED source, Applied Physics B, 101, 661–669, https://doi.org/10.1007/s00340-010-4253-x, http://link.springer.com/10.1007/s00340-010-4253-x, 2010.

Villena, G., Bejan, I., Kurtenbach, R., Wiesen, P., and Kleffmann, J.: Interferences of commercial NO_2 instruments in the urban atmosphere and in a smog chamber, Atmospheric Measurement Techniques, 5, 149–159, https://doi.org/10.5194/amt-5-149-2012, https://www.atmos-meas-tech.net/5/149/2012/, 2012.

Vitousek, P. M., Aber, J. D., Howarth, R. W., Likens, G. E., Matson, P. A., Schindler, D. W., Schlesinger, W. H., and Tilman, D. G.: Human
535   alteration of the global nitrogen cycle: sources and consequences, Ecological Applications, 7, 737–750, https://doi.org/10.1890/1051-
0761(1997)007[0737:HAOTGN]2.0.CO;2, http://doi.wiley.com/10.1890/1051-0761(1997)007[0737:HAOTGN]2.0.CO;2, 1997.

Volkamer, R., Spietz, P., Burrows, J., and Platt, U.: High-resolution absorption cross-section of glyoxal in the UV–vis and IR spectral
ranges, Journal of Photochemistry and Photobiology A: Chemistry, 172, 35–46, https://doi.org/10.1016/j.jphotochem.2004.11.011, https:
//linkinghub.elsevier.com/retrieve/pii/S1010603004005143, 2005.

540   Volkamer, R., San Martini, F., Molina, L. T., Salcedo, D., Jimenez, J. L., and Molina, M. J.: A missing sink for gas-phase glyoxal in
Mexico City: formation of secondary organic aerosol, Geophysical Research Letters, 34, L19 807, https://doi.org/10.1029/2007GL030752,
http://doi.wiley.com/10.1029/2007GL030752, 2007.

Wachsstock, D.: Tenua: the kinetics simulator for Java; http://bililite.com/tenua., http://bililite.com/tenua, 2007.

Wagner, T., Ibrahim, O., Shaiganfar, R., and Platt, U.: Mobile MAX-DOAS observations of tropospheric trace gases, Atmos. Meas. Tech.,
545   p. 12, 2010.

Washenfelder, R. A., Langford, A. O., Fuchs, H., and Brown, S. S.: Measurement of glyoxal using an Incoherent BroadBand Cavity Enhanced
Absorption Spectrometer, Atmos. Chem. Phys., p. 15, 2008.

Werle, P., Mücke, R., and Slemr, F.: The limits of signal averaging in atmospheric trace-gas monitoring by Tunable Diode-Laser Absorption
Spectroscopy (TDLAS), Applied Physics B Photophysics and Laser Chemistry, 57, 131–139, https://doi.org/10.1007/BF00425997, http:
550   //link.springer.com/10.1007/BF00425997, 1993.

Williams, E. J., Baumann, K., Roberts, J. M., Bertman, S. B., Norton, R. B., Fehsenfeld, F. C., Springston, S. R., Nunnermacker, L. J.,
Newman, L., Olszyna, K., Meagher, J., Hartsell, B., Edgerton, E., Pearson, J. R., and Rodgers, M. O.: Intercomparison of ground-based
NO_y measurement techniques, Journal of Geophysical Research: Atmospheres, 103, 22 261–22 280, https://doi.org/10.1029/98JD00074,
http://doi.wiley.com/10.1029/98JD00074, 1998.

555   Wine, P. H. and Nicovich, J. M.: Atmospheric Radical Chemistry, in: Encyclopedia of Radicals in Chemistry, Biology and Materials, edited
by Chatgilialoglu, C. and Studer, A., p. rad015, John Wiley & Sons, Ltd, Chichester, UK, https://doi.org/10.1002/9781119953678.rad015,
http://doi.wiley.com/10.1002/9781119953678.rad015, 2012.

Wittrock, F., Oetjen, H., Richter, A., Fietkau, S., Medeke, T., Rozanov, A., and Burrows, J. P.: MAX-DOAS measurements of atmo-
spheric trace gases in Ny-Ålesund - radiative transfer studies and their application, Atmospheric Chemistry and Physics, 4, 955–966,
560   https://doi.org/10.5194/acp-4-955-2004, http://www.atmos-chem-phys.net/4/955/2004/, 2004.